Noncolocated Time-Reversal MUSIC: High-SNR Distribution of Null Spectrum

Domenico Ciuonzo, *Senior Member, IEEE*, and Pierluigi Salvo Rossi, *Senior Member, IEEE*

***Abstract*—We derive the asymptotic distribution of the null spectrum of the well-known Multiple Signal Classification (MUSIC) in its computational Time-Reversal (TR) form. The result pertains to a single-frequency noncolocated multistatic scenario and several TR-MUSIC variants are investigated here. The analysis builds upon the first-order perturbation of the singular value decomposition and allows a simple characterization of null-spectrum moments (up to the second order). This enables a comparison in terms of spectrums stability. Finally, a numerical analysis is provided to confirm the theoretical findings.**

***Index Terms*—Null-spectrum, radar imaging, resolution, Time-Reversal (TR), TR Multiple Signal Classification (TR-MUSIC).**

I. Introduction

TIME-REVERSAL (TR) refers to all those methods that exploit the invariance of the wave equation (in lossless and stationary media) by re-transmitting a time-reversed version of the scattered (or radiated) field measured by an array to focus on a scattering object (or radiating source), by physical [1] or synthetic [2] means. In the latter case (*computational TR*), it consists in *numerically* backpropagating the field data by using a known Green' s function, representative of the propagation medium. Since the employed Green function depends on the object (or source) position, an image is formed by varying the probed location (this procedure is referred to as "imaging"). Computational TR has been successfully applied in different contexts such as subsurface prospecting [3], through-the-wall [4], and microwave imaging [5].

The key entity in TR-imaging is the Multistatic Data Matrix (MDM), whose entries are the scattered field due to each transmit–receive (Tx–Rx) pair. Two popular methods for TR-imaging are the decomposition of TR operator (DORT) [6] and the TR Multiple Signal Classification (TR-MUSIC) [7]. DORT imaging exploits the MDM spectrum by backpropagating each eigenvector of the so-called *signal subspace*, thus allowing us to selectively focus on each (well-resolved) scatterer. On the other hand, TR-MUSIC imaging is based on a complementary point of view and relies on the *noise subspace* (viz., orthogonal-subspace[1]), leading to satisfactory performance as long as the data space dimension exceeds the signal subspace dimension and sufficiently high signal-to-noise ratio (SNR) is present. TR-MUSIC was first introduced for a Born Approximated (BA) linear scattering model [7] and, later, successfully applied to the Foldy–Lax (FL) nonlinear model [8]. Also, it became popular mainly due to the following reasons:

1) algorithmic efficiency;
2) no need for approximate scattering models;
3) finer resolution than the diffraction limits (especially in scenarios with few scatterers).

Recently, TR-MUSIC has been expanded to extended scatterers in [9].

Although a vast literature on performance analysis of MUSIC [10] for Direction-Of-Arrival (DOA) estimation exists (see [11], [12] for resolution studies and [13]–[16] for asymptotic Mean-Squared-Error (MSE) derivation, with more advanced studies presented in [17]–[19]), such results cannot be directly applied to TR-MUSIC. Indeed, in TR framework scatterers/sources are generally assumed deterministic and more importantly a *single snapshot is used*, whereas MUSIC results for DOA refer to a different asymptotic condition (i.e., a large number of snapshots). Also, to our knowledge, *no corresponding theoretical results have been proposed in the literature* for TR-MUSIC, except for [20] and [21], providing the asymptotic (high-SNR) localization MSE for point-like scatterers. Yet, a few works have tackled achievable performance both for BA and FL models via the Cramér–Rao lower bound [22].

In this letter, we provide a null-spectrum[2] analysis of TR-MUSIC for point-like scatterers, via a first-order perturbation of singular value decomposition (SVD) [24], thus having asymptotic validity (i.e., meaning a high-SNR regime). The present results are based on a homogeneous background assumption and

Manuscript received December 2, 2016; accepted January 24, 2017. Date of publication January 30, 2017; date of current version March 1, 2017. The associate editor coordinating the review of this manuscript and approving it for publication was Dr. P. Venkitasubramaniam.

D. Ciuonzo is with the Networking Measurement and Monitoring S.R.L., Naples 80143, Italy (e-mail: domenico.ciuonzo@gmail.com).

P. Salvo Rossi is with the Department of Electronics and Telecommunications, Norwegian University of Science and Technology, Trondheim Norway (e-mail: salvorossi@ieee.org).

Color versions of one or more of the figures in this letter are available online at http://ieeexplore.ieee.org.

Digital Object Identifier 10.1109/LSP.2017.2661246

Notation - Lower-case (resp. Upper-case) bold letters denote column vectors (resp. matrices), with a_n (resp. $a_{n,m}$) being the nth (resp. the (n,m)th) element of $\boldsymbol{a}$ (resp. $\boldsymbol{A}$); $\mathbb{E}\{\cdot\}, \mathrm{var}\{\cdot\}, (\cdot)^T, (\cdot)^\dagger, (\cdot)^*, \mathrm{Tr}[\cdot], \mathrm{vec}(\cdot), (\cdot)^-$, $\Re(\cdot), \delta(\cdot), \|\cdot\|_F$ and $\|\cdot\|$ denote expectation, variance, transpose, Hermitian, conjugate, matrix trace, vectorization, pseudo-inverse, real part, Kronecker delta, Frobenius and ℓ_2 norm operators, respectively; j denotes the imaginary unit; $\mathbf{0}_{N\times M}$ (resp. $\boldsymbol{I}_N$) denotes the $N\times M$ null (resp. identity) matrix; $\mathbf{0}_N$ (resp. $\mathbf{1}_N$) denotes the null (resp. ones) column vector of length N; $\mathrm{diag}(\boldsymbol{a})$ denotes the diagonal matrix obtained from the vector $\boldsymbol{a}$; $\boldsymbol{x}_{1:M} \triangleq \left[\boldsymbol{x}_1^T \ \cdots \ \boldsymbol{x}_M^T\right]^T$ denotes the vector concatenation; $\mathcal{N}_{\mathbb{C}}(\boldsymbol{\mu}, \boldsymbol{\Sigma})$ denotes a proper complex Gaussian pdf with mean vector $\boldsymbol{\mu}$ and covariance $\boldsymbol{\Sigma}$; $\mathcal{C}\chi^2_N$ denotes a complex chi-square distribution with N (complex) Degrees of Freedom (DOFs); finally the symbol $\sim$ means distributed as.

[1] Such term underlines that it is orthogonal to the signal subspace.

[2] We underline that the MUSIC imaging function is commonly referred to as "pseudo-spectrum" in DOA literature. Although less used, in this letter, we will instead adopt the term "null-spectrum" employed in [23], as the latter work represents the closest counterpart in DOA estimation to the present study.

neglecting mutual coupling, as well as polarization or antenna pattern effects. Here, we build upon [25] (tackling the simpler colocated case) and consider a *general* noncolocated multistatic setup with BA/FL models, where several TR-MUSIC variants, proposed in the literature, are investigated. The obtained results complement those found in DOA literature [23] and allow us to obtain both the mean and the variance of each null-spectrum, as well as to draw-out its probability density function (pdf). Also, they highlight performance dependence of a null-spectrum on the scatterers/arrays configurations and compare TR-MUSIC variants in terms of spectrum stability. We recall that stability property is important for TR-MUSIC, and has been investigated by numerical means [26], [27] or using compressed-sensing-based approaches [28]. Finally, a few numerical examples, for a two-dimensional (2-D) geometry with scalar scattering, are presented to confirm our findings.

The letter is organized as follows: Section II describes the system model and reviews classic results on SVD perturbation analysis. Section III presents the theoretical characterization of TR-MUSIC null-spectrum, whereas its validation is shown in Section IV via simulations. Finally, conclusions are in Section V.

II. System Model

We consider localization of M point-like scatterers[3] at unknown positions $\{\boldsymbol{x}_k\}_{k=1}^{M}$ in $\mathbb{R}^p$ with unknown scattering potentials $\{\tau_k\}_{k=1}^{M}$ in $\mathbb{C}$. The Tx (resp. Rx) array consists of N_T (resp. N_R) isotropic point elements (resp. receivers) located at $\{\tilde{\boldsymbol{r}}_i\}_{i=1}^{N_T}$ in $\mathbb{R}^p$ (resp. $\{\bar{\boldsymbol{r}}_j\}_{j=1}^{N_R}$ in $\mathbb{R}^p$). The illuminators first send signals to the probed scenario (in a known homogeneous background with wavenumber κ) and the transducer array records the received signals. The (single-frequency) measurement model is then [30]:

$$\boldsymbol{K}_n = \boldsymbol{K}(\boldsymbol{x}_{1:M}, \boldsymbol{\tau}) + \boldsymbol{W} \quad (1)$$

$$= \boldsymbol{G}_{\mathrm{r}}(\boldsymbol{x}_{1:M})\, \boldsymbol{M}(\boldsymbol{x}_{1:M}, \boldsymbol{\tau})\, \boldsymbol{G}_{\mathrm{t}}(\boldsymbol{x}_{1:M})^T + \boldsymbol{W} \quad (2)$$

where $\boldsymbol{K}_n \in \mathbb{C}^{N_R \times N_T}$ (resp. $\boldsymbol{K}(\boldsymbol{x}_{1:M}, \boldsymbol{\tau})$) denotes the measured (resp. noise-free) MDM. Differently $\boldsymbol{W} \in \mathbb{C}^{N_R \times N_T}$ is a noise matrix s.t. $\mathrm{vec}(\boldsymbol{W}) \sim \mathcal{N}_{\mathbb{C}}(\boldsymbol{0}_N, \sigma_w^2\, \boldsymbol{I}_N)$, where $N \triangleq N_T N_R$. Additionally, we have denoted: 1) the vector of scattering coefficients as $\boldsymbol{\tau} \triangleq [\,\tau_1 \,\cdots\, \tau_M\,]^T \in \mathbb{C}^{M\times 1}$; 2) the Tx (resp. Rx) array matrix as $\boldsymbol{G}_{\mathrm{t}}(\boldsymbol{x}_{1:M}) \in \mathbb{C}^{N_T \times M}$ (resp. $\boldsymbol{G}_{\mathrm{r}}(\boldsymbol{x}_{1:M}) \in \mathbb{C}^{N_R \times M}$), whose (i,j)th entry equals $\mathcal{G}(\tilde{\boldsymbol{r}}_i, \boldsymbol{x}_j)$ (resp. $\mathcal{G}(\bar{\boldsymbol{r}}_i, \boldsymbol{x}_j)$), where $\mathcal{G}(\cdot,\cdot)$ denotes the (scalar) background *Green function*[7]. Also, the jth column $\boldsymbol{g}_{\mathrm{t}}(\boldsymbol{x}_j)$ (resp. $\boldsymbol{g}_{\mathrm{r}}(\boldsymbol{x}_j)$) of $\boldsymbol{G}_{\mathrm{t}}(\boldsymbol{x}_{1:M})$ (resp. $\boldsymbol{G}_{\mathrm{r}}(\boldsymbol{x}_{1:M})$) denotes the Tx (resp. Rx) Green's function vector evaluated at $\boldsymbol{x}_j$. In (2), the scattering matrix $\boldsymbol{M}(\boldsymbol{x}_{1:M}, \boldsymbol{\tau}) \in \mathbb{C}^{M\times M}$ equals $\boldsymbol{M}(\boldsymbol{x}_{1:M}, \boldsymbol{\tau}) \triangleq \mathrm{diag}(\boldsymbol{\tau})$ for the BA model [7], while $\boldsymbol{M}(\boldsymbol{x}_{1:M}, \boldsymbol{\tau}) \triangleq [\mathrm{diag}^{-1}(\boldsymbol{\tau}) - \boldsymbol{S}(\boldsymbol{x}_{1:M})]^{-1}$ in the case of the FL model [22], where the (m,n)th entry of $\boldsymbol{S}(\boldsymbol{x}_{1:M})$ equals $\mathcal{G}(\boldsymbol{x}_m, \boldsymbol{x}_n)$ when $m \neq n$ and zero otherwise. We recall that our null-spectrum analysis of TR-MUSIC *is general* and can be applied to both scattering models.

Finally, we define the $\mathrm{SNR} \triangleq \|\boldsymbol{K}(\boldsymbol{x}_{1:M}, \boldsymbol{\tau})\|_F^2 / (\sigma_w^2\, N_T N_R)$ and, for notational convenience, $N_{\mathrm{Rdof}} \triangleq (N_R - M)$ and $N_{\mathrm{Tdof}} \triangleq (N_T - M)$ as the dimensions of the left and right orthogonal subspaces, whereas $N_{\mathrm{dof}} \triangleq (N_{\mathrm{Rdof}} + N_{\mathrm{Tdof}})$.

[3]The number of scatterers M is assumed to be known, as usually done in array-processing literature [29].

A. TR-MUSIC Spatial Spectrum

Several TR-MUSIC variants have been proposed in the literature for the non colocated setup [8]. A first approach consists in using the so-called *Rx mode TR-MUSIC*, which evaluates the *null (or spatial) spectrum* (assuming $M < N_R$):

$$\mathcal{P}_{\mathrm{r}}(\boldsymbol{x}; \widetilde{\boldsymbol{U}}_n) \triangleq \bar{\boldsymbol{g}}_r(\boldsymbol{x})^{\dagger}\, \widetilde{\boldsymbol{P}}_{\mathrm{r},n}\, \bar{\boldsymbol{g}}_r(\boldsymbol{x}) = \left\| \widetilde{\boldsymbol{U}}_n^{\dagger}\, \bar{\boldsymbol{g}}_r(\boldsymbol{x}) \right\|^2 \quad (3)$$

where $\widetilde{\boldsymbol{U}}_n \in \mathbb{C}^{N_R \times N_{\mathrm{Rdof}}}$ is the matrix of left singular vectors of $\boldsymbol{K}_n$ spanning the noise subspace, $\bar{\boldsymbol{g}}_{\mathrm{r}}(\boldsymbol{x}) \triangleq \boldsymbol{g}_{\mathrm{r}}(\boldsymbol{x}) / \|\boldsymbol{g}_{\mathrm{r}}(\boldsymbol{x})\|$ is the unit-norm Rx Green vector function and $\widetilde{\boldsymbol{P}}_{\mathrm{r},n} \triangleq (\widetilde{\boldsymbol{U}}_n \widetilde{\boldsymbol{U}}_n^{\dagger})$ (i.e., the "noisy" projector into the left noise subspace). A dual approach, denoted as *Tx mode TR-MUSIC*, constructs the null spectrum (assuming $M < N_T$):

$$\mathcal{P}_{\mathrm{t}}(\boldsymbol{x}; \widetilde{\boldsymbol{V}}_n) \triangleq \bar{\boldsymbol{g}}_{\mathrm{t}}(\boldsymbol{x})^{T}\, \widetilde{\boldsymbol{P}}_{\mathrm{t},n}\, \bar{\boldsymbol{g}}_{\mathrm{t}}(\boldsymbol{x})^{*} = \left\| \widetilde{\boldsymbol{V}}_n^{\dagger}\, \bar{\boldsymbol{g}}_{\mathrm{t}}^{*}(\boldsymbol{x}) \right\|^2 \quad (4)$$

where $\widetilde{\boldsymbol{V}}_n \in \mathbb{C}^{N_T \times N_{\mathrm{Tdof}}}$ is the matrix of right singular vectors of $\boldsymbol{K}_n$ spanning the noise subspace, $\bar{\boldsymbol{g}}_{\mathrm{t}}(\boldsymbol{x}) \triangleq \boldsymbol{g}_{\mathrm{t}}(\boldsymbol{x}) / \|\boldsymbol{g}_{\mathrm{t}}(\boldsymbol{x})\|$ is the unit-norm Tx Green vector function and $\widetilde{\boldsymbol{P}}_{\mathrm{t},n} \triangleq (\widetilde{\boldsymbol{V}}_n \widetilde{\boldsymbol{V}}_n^{\dagger})$ (i.e., the "noisy" projector into the right noise subspace). Finally, a combined version of two modes, named *generalized TR-MUSIC,* is built as (assuming $M < \min\{N_T, N_R\}$) [8]:

$$\mathcal{P}_{\mathrm{tr}}(\boldsymbol{x}; \widetilde{\boldsymbol{U}}_n, \widetilde{\boldsymbol{V}}_n) \triangleq \mathcal{P}_{\mathrm{t}}(\boldsymbol{x}; \widetilde{\boldsymbol{V}}_n) + \mathcal{P}_{\mathrm{r}}(\boldsymbol{x}; \widetilde{\boldsymbol{U}}_n). \quad (5)$$

Usually, the M largest local maxima of $\mathcal{P}_{\mathrm{r}}(\boldsymbol{x}; \widetilde{\boldsymbol{U}}_n)^{-1}$, $\mathcal{P}_{\mathrm{t}}(\boldsymbol{x}; \widetilde{\boldsymbol{V}}_n)^{-1}$ and $\mathcal{P}_{\mathrm{tr}}(\boldsymbol{x}; \widetilde{\boldsymbol{U}}_n, \widetilde{\boldsymbol{V}}_n)^{-1}$ are chosen as the estimates $\{\hat{\boldsymbol{x}}_k\}_{k=1}^{M}$. Indeed, it can be shown that (3) (resp. (4)) equals zero when $\boldsymbol{x}$ equals one among $\{\boldsymbol{x}_k\}_{k=1}^{M}$ in the noise-free case, since when $\widetilde{\boldsymbol{U}}_n = \boldsymbol{U}_n$ (resp. $\widetilde{\boldsymbol{V}}_n = \boldsymbol{V}_n$) this reduces to the eigenvector matrix spanning the left (resp. right) noise subspace of $\boldsymbol{K}(\boldsymbol{x}_{1:M}, \boldsymbol{\tau})$ [7]. Similar conclusions hold for $\mathcal{P}_{\mathrm{tr}}(\boldsymbol{x}; \widetilde{\boldsymbol{U}}_n, \widetilde{\boldsymbol{V}}_n)$ in a noise-free condition.

B. Review of Results on SVD Perturbation

We consider a rank deficient matrix $\boldsymbol{A} \in \mathbb{C}^{R\times T}$ with rank $\delta < \min\{R, T\}$, whose SVD $\boldsymbol{A} = \boldsymbol{U}\, \boldsymbol{\Sigma}\, \boldsymbol{V}^{\dagger}$ is rewritten as

$$\boldsymbol{A} = (\,\boldsymbol{U}_s\ \boldsymbol{U}_n\,) \begin{pmatrix} \boldsymbol{\Sigma}_s & \boldsymbol{0}_{\delta\times\check{\delta}} \\ \boldsymbol{0}_{\bar{\delta}\times\delta} & \boldsymbol{0}_{\bar{\delta}\times\check{\delta}} \end{pmatrix} \begin{pmatrix} \boldsymbol{V}_s^{\dagger} \\ \boldsymbol{V}_n^{\dagger} \end{pmatrix} \quad (6)$$

where $\bar{\delta} \triangleq (R - \delta)$ and $\check{\delta} \triangleq (T - \delta)$, respectively. Also, $\boldsymbol{U}_s \in \mathbb{C}^{R\times\delta}$ and $\boldsymbol{V}_s \in \mathbb{C}^{T\times\delta}$ (resp. $\boldsymbol{U}_n \in \mathbb{C}^{R\times\bar{\delta}}$ and $\boldsymbol{V}_n \in \mathbb{C}^{T\times\check{\delta}}$) denote the left and right singular vectors of signal (resp. orthogonal) subspaces in (6), while $\boldsymbol{\Sigma}_s \in \mathbb{R}^{\delta\times\delta}$ collects the (>0) singular values of the signal subspace. Then, consider $\widetilde{\boldsymbol{A}} = (\boldsymbol{A} + \boldsymbol{N})$, where $\boldsymbol{N}$ is a perturbing term. Similarly to (6), the SVD $\widetilde{\boldsymbol{A}} = \widetilde{\boldsymbol{U}}\widetilde{\boldsymbol{\Sigma}}\widetilde{\boldsymbol{V}}^{\dagger}$ is rewritten as

$$\widetilde{\boldsymbol{A}} = (\,\widetilde{\boldsymbol{U}}_s\ \widetilde{\boldsymbol{U}}_n\,) \begin{pmatrix} \widetilde{\boldsymbol{\Sigma}}_s & \boldsymbol{0}_{\delta\times\check{\delta}} \\ \boldsymbol{0}_{\bar{\delta}\times\delta} & \widetilde{\boldsymbol{\Sigma}}_n \end{pmatrix} \begin{pmatrix} \widetilde{\boldsymbol{V}}_s^{\dagger} \\ \widetilde{\boldsymbol{V}}_n^{\dagger} \end{pmatrix} \quad (7)$$

showing the effect of $\boldsymbol{N}$ on the spectral representation[4] of $\widetilde{\boldsymbol{A}}$, highlighting the change of the left and right principal directions. We are here concerned with the perturbations pertaining to $\widetilde{\boldsymbol{U}}_n$ and $\widetilde{\boldsymbol{V}}_n$, stressed as $\widetilde{\boldsymbol{U}}_n = \boldsymbol{U}_n + \boldsymbol{\Delta U}_n$ and

[4]Indeed, as opposed to (6), $\widetilde{\boldsymbol{A}}$ may be full-rank in general.

$\widetilde{\boldsymbol{V}}_n = \boldsymbol{V}_n + \boldsymbol{\Delta V}_n$, where $\boldsymbol{\Delta}(\cdot)$ terms are generally complicated functions of $\boldsymbol{N}$. However, when $\boldsymbol{N}$ has a "small magnitude" compared to $\boldsymbol{A}$ (see [31]), a first-order perturbation (i.e., $\boldsymbol{\Delta}(\cdot)$ are approximated as linear with $\boldsymbol{N}$), will be accurate [24]. The key result is that perturbed orthogonal left subspace $\widetilde{\boldsymbol{U}}_n$ (resp. right subspace $\widetilde{\boldsymbol{V}}_n$) is spanned by $\boldsymbol{U}_n + \boldsymbol{U}_s\boldsymbol{B}$ (resp. $\boldsymbol{V}_n + \boldsymbol{V}_s\bar{\boldsymbol{B}}$), where norm (any submultiplicative one, such as ℓ_2 or $\|\cdot\|_F$ norm) of $\boldsymbol{B}$ (resp. $\bar{\boldsymbol{B}}$) is of the same order of that of $\boldsymbol{N}$. Intuitively, a *small perturbation* is observed at *high-SNR*. The expressions for $\boldsymbol{\Delta U}_n$ and $\boldsymbol{\Delta V}_n$, at first order, are[5] [32]

$$\boldsymbol{\Delta U}_n = -(\boldsymbol{A}^{-})^{\dagger}\,\boldsymbol{N}^{\dagger}\,\boldsymbol{U}_n; \quad \boldsymbol{\Delta V}_n = -(\boldsymbol{A}^{-})\,\boldsymbol{N}\,\boldsymbol{V}_n \quad (8)$$

where we have exploited $\boldsymbol{A}^{-} = \boldsymbol{V}_s\,\boldsymbol{\Sigma}_s^{-1}\,\boldsymbol{U}_s^{\dagger}$ [33].

III. Null-Spectrum Analysis

First, we observe that the null spectrums at scatterer positions $\mathcal{P}_{\rm r}(\boldsymbol{x}_k;\widetilde{\boldsymbol{U}}_n)$, $\mathcal{P}_{\rm t}(\boldsymbol{x}_k;\widetilde{\boldsymbol{V}}_n)$ and $\mathcal{P}_{\rm tr}(\boldsymbol{x}_k;\widetilde{\boldsymbol{U}}_n,\widetilde{\boldsymbol{V}}_n)$, $k\in\{1,\ldots,M\}$, in (3), (4), and (5) can be simplified, using $\widetilde{\boldsymbol{U}}_n = \boldsymbol{U}_n + \boldsymbol{\Delta U}_n$ and $\widetilde{\boldsymbol{V}}_n = \boldsymbol{V}_n + \boldsymbol{\Delta V}_n$ and exploiting the properties[6] $\boldsymbol{U}_n^{\dagger}\,\bar{\boldsymbol{g}}_{\rm r}(\boldsymbol{x}_k) = \boldsymbol{0}_{N_{\rm Rdof}}$ and $\boldsymbol{V}_n^{\dagger}\bar{\boldsymbol{g}}_{\rm t}^{*}(\boldsymbol{x}_k) = \boldsymbol{0}_{N_{\rm Tdof}}$, as

$$\mathcal{P}_{\rm r}(\boldsymbol{x}_k;\widetilde{\boldsymbol{U}}_n) = \|\boldsymbol{\xi}_{{\rm r},k}\|^2\,, \quad \mathcal{P}_{\rm t}(\boldsymbol{x}_k;\widetilde{\boldsymbol{V}}_n) = \|\boldsymbol{\xi}_{{\rm t},k}\|^2 \quad (9)$$

where $\boldsymbol{\xi}_{{\rm r},k} \triangleq \boldsymbol{\Delta U}_n^{\dagger}\,\bar{\boldsymbol{g}}_{\rm r}(\boldsymbol{x}_k) \in \mathbb{C}^{N_{\rm Rdof}\times 1}$ and $\boldsymbol{\xi}_{{\rm t},k} \triangleq \boldsymbol{\Delta V}_n^{\dagger}\,\bar{\boldsymbol{g}}_t^{*}(\boldsymbol{x}_k) \in \mathbb{C}^{N_{\rm Tdof}\times 1}$, respectively. Similarly,

$$\mathcal{P}_{\rm tr}(\boldsymbol{x}_k;\widetilde{\boldsymbol{U}}_n,\widetilde{\boldsymbol{V}}_n) = \|\boldsymbol{\xi}_{{\rm t},k}\|^2 + \|\boldsymbol{\xi}_{{\rm r},k}\|^2 = \|\boldsymbol{\xi}_k\|^2 \quad (10)$$

where $\boldsymbol{\xi}_k \triangleq \left[\,\boldsymbol{\xi}_{{\rm r},k}^T\;\boldsymbol{\xi}_{{\rm t},k}^T\,\right]^T \in \mathbb{C}^{N_{\rm dof}\times 1}$. Thus, to characterize $\mathcal{P}_{\rm r}(\boldsymbol{x}_k;\widetilde{\boldsymbol{U}}_n)$, $\mathcal{P}_{\rm t}(\boldsymbol{x}_k;\widetilde{\boldsymbol{V}}_n)$ and $\mathcal{P}_{\rm tr}(\boldsymbol{x}_k;\widetilde{\boldsymbol{U}}_n,\widetilde{\boldsymbol{V}}_n)$, it suffices to study the random vector $\boldsymbol{\xi}_k$. Indeed, the marginal pdfs of $\boldsymbol{\xi}_{{\rm r},k}$ and $\boldsymbol{\xi}_{{\rm t},k}$ are easily drawn from that of $\boldsymbol{\xi}_k$. As a byproduct, $\boldsymbol{\xi}_k$ definition also allows an elegant and simpler MSE analysis with respect to [21], as it can be shown that the position error of the estimates with Tx mode ($\boldsymbol{\Delta x}_{T,k}$), Rx mode ($\boldsymbol{\Delta x}_{R,k}$) and generalized ($\boldsymbol{\Delta x}_{TR,k}$) TR-MUSIC can be expressed as $\boldsymbol{\Delta x}_{T,k} \approx -\boldsymbol{\Gamma}_{T,k}^{-1}\Re\{\boldsymbol{J}_{T,k}^{T}\,\boldsymbol{V}_n\,\boldsymbol{\xi}_{{\rm t},k}\}$, $\boldsymbol{\Delta x}_{R,k} \approx -\boldsymbol{\Gamma}_{R,k}^{-1}\Re\{\boldsymbol{J}_{R,k}^{\dagger}\,\boldsymbol{U}_n\,\boldsymbol{\xi}_{{\rm r},k}\}$ and $\boldsymbol{\Delta x}_{TR,k} \approx -\boldsymbol{\Gamma}_{TR,k}^{-1}\Re\{[\,(\boldsymbol{J}_{R,k}^{\dagger}\,\boldsymbol{U}_n)\;(\boldsymbol{J}_{T,k}^{T}\,\boldsymbol{V}_n)\,]\boldsymbol{\xi}_k\}$, respectively, where $\boldsymbol{J}_{T,k}$, $\boldsymbol{J}_{R,k}$, $\boldsymbol{\Gamma}_{T,k}$, $\boldsymbol{\Gamma}_{R,k}$, and $\boldsymbol{\Gamma}_{TR,k}$ are suitably defined *known* matrices (see [21]). Clearly, finding the exact pdf of $\boldsymbol{\xi}_k$ is hard, as $\boldsymbol{\Delta U}_n$ and $\boldsymbol{\Delta V}_n$ are generally complicated functions of the unknown *perturbing* matrix $\boldsymbol{W}$.

However, $\boldsymbol{\Delta U}_n$ and $\boldsymbol{\Delta V}_n$ assume a (tractable) closed form with a first-order approximation (see (8)). This approximation holds tightly at high-SNR, as $\boldsymbol{W}$ will be statistically "small" compared to noise-free MDM $\boldsymbol{K}(\boldsymbol{x}_{1:M},\boldsymbol{\tau})$. Hence, at high-SNR, $\boldsymbol{\xi}_k$ is (approximately) expressed in terms of $\boldsymbol{W}$ as

$$\boldsymbol{\xi}_k = \begin{bmatrix}\boldsymbol{\xi}_{{\rm r},k}\\ \boldsymbol{\xi}_{{\rm t},k}\end{bmatrix} \approx \begin{bmatrix}-\boldsymbol{U}_n^{\dagger}\,\boldsymbol{W}\,\boldsymbol{t}_{{\rm r},k}\\ -\boldsymbol{V}_n^{\dagger}\,\boldsymbol{W}^{\dagger}\,\boldsymbol{t}_{{\rm t},k}\end{bmatrix} \quad (11)$$

where $\boldsymbol{t}_{{\rm r},k} \triangleq \boldsymbol{K}^{-}(\boldsymbol{x}_{1:M},\boldsymbol{\tau})\,\bar{\boldsymbol{g}}_{\rm r}(\boldsymbol{x}_k) \in \mathbb{C}^{N_T\times 1}$ and $\boldsymbol{t}_{{\rm t},k} \triangleq \boldsymbol{K}^{-}(\boldsymbol{x}_{1:M},\boldsymbol{\tau})^{\dagger}\,\bar{\boldsymbol{g}}_{\rm t}^{*}(\boldsymbol{x}_k) \in \mathbb{C}^{N_R\times 1}$ are *deterministic*. Since the vector $\boldsymbol{\xi}_k$ is linear[7] with the noise matrix $\boldsymbol{W}$, it will be Gaussian distributed; thus, we only need to evaluate its moments up to the second order to characterize it completely. Hereinafter, we only sketch the main steps and provide the detailed proof as supplementary material. First, the mean vector $\mathbb{E}\{[\,\boldsymbol{\xi}_{{\rm r},k}^T\;\boldsymbol{\xi}_{{\rm t},k}^T\,]^T\} = \boldsymbol{0}_{N_{\rm dof}}$, exploiting $\mathbb{E}\{\boldsymbol{W}\} = \boldsymbol{0}_{N_R\times N_T}$. Secondly, the *covariance matrix* $\boldsymbol{\Xi}_k \triangleq \mathbb{E}\{\boldsymbol{\xi}_k\boldsymbol{\xi}_k^{\dagger}\}$ (since $\mathbb{E}\{\boldsymbol{\xi}_k\} = \boldsymbol{0}_{N_{\rm dof}}$) is given in closed-form as

$$\boldsymbol{\Xi}_k = \begin{bmatrix}\sigma_w^2\,\|\boldsymbol{t}_{{\rm r},k}\|^2\,\boldsymbol{I}_{N_{\rm Rdof}} & \boldsymbol{0}_{N_{\rm Rdof}\times N_{\rm Tdof}}\\ \boldsymbol{0}_{N_{\rm Tdof}\times N_{\rm Rdof}} & \sigma_w^2\,\|\boldsymbol{t}_{{\rm t},k}\|^2\,\boldsymbol{I}_{N_{\rm Tdof}}\end{bmatrix}. \quad (12)$$

The above result is based on circularity of the entries of $\boldsymbol{W}$, along with their mutual independence. Thirdly, aiming at completing the statistical characterization, we evaluate the *pseudo-covariance matrix* $\boldsymbol{\Psi}_k \triangleq \mathbb{E}\{\boldsymbol{\xi}_k\boldsymbol{\xi}_k^{T}\}$ (since $\mathbb{E}\{\boldsymbol{\xi}_k\} = \boldsymbol{0}_{N_{\rm dof}}$), whose closed form is $\boldsymbol{\Psi}_k = \boldsymbol{0}_{N_{\rm dof}\times N_{\rm dof}}$. The latter result is based on circularity of the entries of $\boldsymbol{W}$, along with their mutual independence and exploiting the results $\boldsymbol{V}_n^{\dagger}\,\boldsymbol{t}_{{\rm r},k} = \boldsymbol{0}_{N_{\rm Tdof}}$ and $\boldsymbol{U}_n^{\dagger}\,\boldsymbol{t}_{\rm t,k} = \boldsymbol{0}_{N_{\rm Rdof}}$, arising from subspaces orthogonality $\boldsymbol{V}_n^{\dagger}\boldsymbol{V}_s = \boldsymbol{0}_{N_{\rm Tdof}\times M}$ and $\boldsymbol{U}_n^{\dagger}\boldsymbol{U}_s = \boldsymbol{0}_{N_{\rm Rdof}\times M}$.

Therefore, in summary $\boldsymbol{\xi}_k \sim \mathcal{N}_{\mathbb{C}}(\boldsymbol{0}_{N_{\rm dof}},\,\boldsymbol{\Xi}_k)$, i.e., a *proper* complex Gaussian vector [34]. Similarly, it is readily inferred that $\boldsymbol{\xi}_{{\rm r},k} \sim \mathcal{N}_{\mathbb{C}}(\boldsymbol{0}_{N_{\rm Rdof}},\,\sigma_w^2\,\|\boldsymbol{t}_{{\rm r},k}\|^2\,\boldsymbol{I}_{N_{\rm Rdof}})$ and $\boldsymbol{\xi}_{{\rm t},k} \sim \mathcal{N}_{\mathbb{C}}(\boldsymbol{0}_{N_{\rm Tdof}},\,\sigma_w^2\,\|\boldsymbol{t}_{{\rm t},k}\|^2\,\boldsymbol{I}_{N_{\rm Tdof}})$, respectively, i.e., they are *independent proper* Gaussian vectors. Clearly, since $\boldsymbol{\xi}_{{\rm r},k}$ and $\boldsymbol{\xi}_{t,k}$ have zero mean and scaled-identity covariance, the corresponding *variance-normalized* energies $\|\boldsymbol{\xi}_{{\rm r},k}\|^2/(\sigma_w^2\|\boldsymbol{t}_{{\rm r},k}\|^2) \sim \mathcal{C}\chi^2_{N_{\rm Rdof}}$ and $\|\boldsymbol{\xi}_{{\rm t},k}\|^2/(\sigma_w^2\|\boldsymbol{t}_{{\rm t},k}\|^2) \sim \mathcal{C}\chi^2_{N_{\rm Tdof}}$, respectively (i.e., they are chi-square distributed). Interestingly, these DOFs coincide with those available for TR-MUSIC localization through Rx and Tx modes, respectively.

Based on these considerations, the means of the null-spectrum for Tx and Rx modes are $\mathbb{E}\{\|\boldsymbol{\xi}_{{\rm r},k}\|^2\} = \sigma_w^2\,\|\boldsymbol{t}_{{\rm r},k}\|^2\,N_{\rm Rdof}$ and $\mathbb{E}\{\|\boldsymbol{\xi}_{{\rm t},k}\|^2\} = \sigma_w^2\,\|\boldsymbol{t}_{{\rm t},k}\|^2\,N_{\rm Tdof}$, respectively, whereas for generalized null-spectrum $\mathbb{E}\{\|\boldsymbol{\xi}_k\|^2\} = \mathbb{E}\{\|\boldsymbol{\xi}_{{\rm r},k}\|^2\} + \mathbb{E}\{\|\boldsymbol{\xi}_{{\rm t},k}\|^2\}$ (by linearity). By similar reasoning, the variances for Tx and Rx modes are given by $\mathrm{var}\{\|\boldsymbol{\xi}_{{\rm r},k}\|^2\} = \sigma_w^4\,\|\boldsymbol{t}_{{\rm r},k}\|^4\,N_{\rm Rdof}$ and $\mathrm{var}\{\|\boldsymbol{\xi}_{{\rm t},k}\|^2\} = \sigma_w^4\,\|\boldsymbol{t}_{{\rm t},k}\|^4\,N_{\rm Tdof}$, respectively, whereas for the generalized null-spectrum $\mathrm{var}\{\|\boldsymbol{\xi}_k\|^2\} = \mathrm{var}\{\|\boldsymbol{\xi}_{{\rm r},k}\|^2\} + \mathrm{var}\{\|\boldsymbol{\xi}_{{\rm t},k}\|^2\}$ (by independence of $\boldsymbol{\xi}_{{\rm r},k}$ and $\boldsymbol{\xi}_{{\rm t},k}$).

Hence, once we have obtained the mean and the variance of $\mathcal{P}_{\rm r}(\boldsymbol{x}_k;\widetilde{\boldsymbol{U}}_n)$, $\mathcal{P}_{\rm t}(\boldsymbol{x}_k;\widetilde{\boldsymbol{V}}_n)$ and $\mathcal{P}_{\rm tr}(\boldsymbol{x}_k;\widetilde{\boldsymbol{U}}_n,\widetilde{\boldsymbol{V}}_n)$, respectively, we can consider the *Normalized Standard Deviation* (NSD), generically defined as

$$\mathrm{NSD}_k \triangleq \sqrt{\mathrm{var}\{\mathcal{P}(\boldsymbol{x}_k;\,\cdot)\}}\,/\,\mathbb{E}\{\mathcal{P}(\boldsymbol{x}_k;\,\cdot)\}. \quad (13)$$

Clearly, the lower the NSD, the higher the null-spectrum stability at $\boldsymbol{x}_k$ [23]. For *Rx* and *Tx modes*, it follows that $\mathrm{NSD}_{{\rm r},k} = 1/\sqrt{N_{\rm Rdof}}$ and $\mathrm{NSD}_{{\rm t},k} = 1/\sqrt{N_{\rm Tdof}}$, respectively. It is apparent that in both cases the NSD *does not depend* (at high-SNR) on the scatterers and measurement setup, as well as σ_w^2, but only on the (complex) DOFs, being equal to $N_{\rm Rdof}$ and $N_{\rm Tdof}$, respectively. Thus, the NSD becomes (asymptotically) small only when the number of scatterers is few compared to the Tx (resp. Rx) elements of the array. Those results are analogous to the case of MUSIC null-spectrum for DOA, whose NSD

[5]We notice that in obtaining (8), "in-space" perturbations (e.g., the contribution to $\boldsymbol{\Delta U}_n$ depending on $\boldsymbol{U}_n$) are not considered, though they have been shown to be linear with $\boldsymbol{N}$ (and thus *not negligible* at first order) [32]. The reason is that these terms do not affect performance analysis of TR-MUSIC null-spectrum when evaluated at scatterers positions $\{\boldsymbol{x}_k\}_{k=1}^{M}$, due to the null spectrum orthogonality property.

[6]Such conditions directly follow from orthogonality between left (resp. right) signal and orthogonal subspaces $\boldsymbol{U}_s$ and $\boldsymbol{U}_n$ (resp. $\boldsymbol{V}_s$ and $\boldsymbol{V}_n$).

[7]In the following of the letter, we will implicitly mean that the results hold "approximately" in the high-SNR regime.

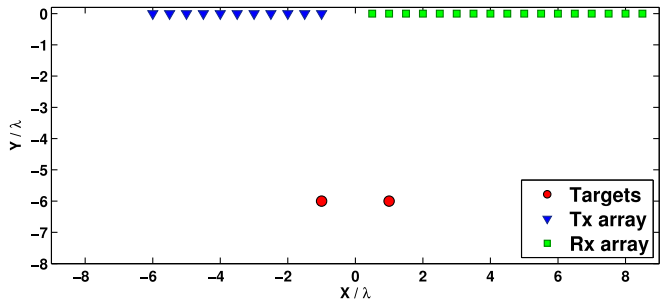

Fig. 1. Geometry for the considered imaging problem in 2-D space.

depends on the DOFs, namely the difference between the (Rx) array size and the number of sources [23]. Differently, the NSD for generalized TR-MUSIC null spectrum equals

$$\mathrm{NSD}_k = \frac{\sqrt{\|\boldsymbol{t}_{\mathrm{r},k}\|^4 N_{\mathrm{Rdof}} + \|\boldsymbol{t}_{\mathrm{t},k}\|^4 N_{\mathrm{Tdof}}}}{\|\boldsymbol{t}_{\mathrm{r},k}\|^2 N_{\mathrm{Rdof}} + \|\boldsymbol{t}_{\mathrm{t},k}\|^2 N_{\mathrm{Tdof}}}. \tag{14}$$

Equation (14) underlines 1) a clear dependence of generalized null-spectrum NSD on scatterers and measurement setup and 2) independence from the noise level σ_w^2. Also, it is apparent that when $\|\boldsymbol{t}_{\mathrm{r},k}\| \approx 0$ (resp. $\|\boldsymbol{t}_{\mathrm{t},k}\| \approx 0$) the expression reduces to $\mathrm{NSD}_k \approx 1/\sqrt{N_{\mathrm{Tdof}}}$ (resp. $\mathrm{NSD}_k \approx 1/\sqrt{N_{\mathrm{Rdof}}}$), i.e., the NSD is *dominated* by Tx (resp. Rx) mode stability. Finally, the same equation is exploited to obtain the conditions ensuring that generalized TR-MUSIC spectrum is "more stable" than Tx and Rx modes ($\mathrm{NSD}_k \leq \mathrm{NSD}_{\mathrm{t},k}$ and $\mathrm{NSD}_k \leq \mathrm{NSD}_{\mathrm{r},k}$, respectively), expressed as the pair of inequalities

$$\begin{cases} \frac{1}{2}\left[1 - N_{\mathrm{Rdof}}/N_{\mathrm{Tdof}}\right] \leq \left(\|\boldsymbol{t}_{\mathrm{t},k}\| \,/\, \|\boldsymbol{t}_{\mathrm{r},k}\|\right)^2 & (\mathrm{Tx}) \\ \frac{1}{2}\left[1 - N_{\mathrm{Tdof}}/N_{\mathrm{Rdof}}\right] \leq \left(\|\boldsymbol{t}_{\mathrm{r},k}\| \,/\, \|\boldsymbol{t}_{\mathrm{t},k}\|\right)^2 & (\mathrm{Rx}). \end{cases} \tag{15}$$

Clearly, when $N_R > N_T$ (resp. $N_T > N_R$) the inequality regarding the Tx (resp. Rx) mode is always verified as the left-hand side is always negative. Also, in the special case $N_T = N_R$ the left-hand side is always zero for both inequalities.

IV. Numerical Results

In this section, we confirm our findings through simulations, focusing on 2-D localization, with Green's function[8] being $\mathcal{G}(\boldsymbol{x}', \boldsymbol{x}) = H_0^{(1)}(\kappa\|\boldsymbol{x}' - \boldsymbol{x}\|)$. Here, $H_n^{(1)}(\cdot)$ and $\kappa = 2\pi/\lambda$ denote the nth order *Hankel* function of the first kind and the wavenumber (λ is the wavelength), respectively. First, we consider a setup with $\lambda/2$-spaced Tx/Rx arrays ($N_T = 11$ and $N_R = 17$, respectively, see Fig. 1). Secondly, to quantify the level of multiple scattering (as in [8]), we define the index $\eta \triangleq \|\boldsymbol{K}_{\mathrm{f}}(\boldsymbol{x}_{1:M}, \boldsymbol{\tau}) - \boldsymbol{K}_{\mathrm{b}}(\boldsymbol{x}_{1:M}, \boldsymbol{\tau})\|_F / \|\boldsymbol{K}_{\mathrm{b}}(\boldsymbol{x}_{1:M}, \boldsymbol{\tau})\|_F$, where $\boldsymbol{K}_{\mathrm{b}}(\boldsymbol{x}_{1:M}, \boldsymbol{\tau})$ and $\boldsymbol{K}_{\mathrm{f}}(\boldsymbol{x}_{1:M}, \boldsymbol{\tau})$ denote the MDMs generated via BA and FL models, respectively. Finally, for simplicity we consider $M = 2$ targets located at $(\boldsymbol{x}_1/\lambda) = [-1 \ -6]^T$ and $(\boldsymbol{x}_2/\lambda) = [+1 \ -6]^T$ and having scattering coefficients $\boldsymbol{\tau} = [3 \ 4]^T$; thus, $\eta = (0.7445)$.

Then, we compare the asymptotic NSD ((14), solid lines) with the true ones obtained via Monte Carlo (MC) simulation (dashed lines, 10^5 runs), focusing only on the generalized null-spectrum for brevity. To this end, Fig. 2 depicts the null-spectrum NSD

[8]We discard the irrelevant constant term $j/4$.

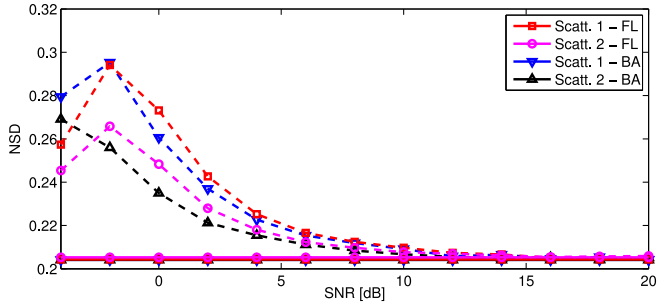

Fig. 2. NSD (generalized null spectrum) versus SNR; theoretical ((14), solid lines) versus MC-based (dashed lines) performance.

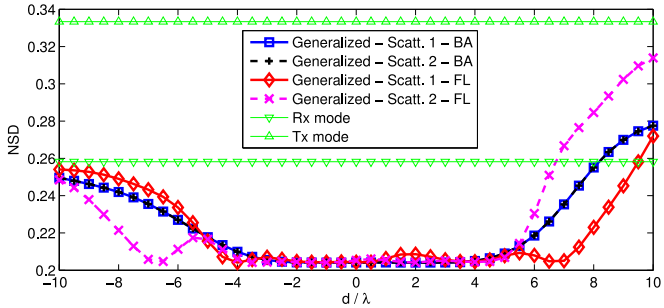

Fig. 3. Theoretical NSD versus scatterers rigid shift d; two targets located at $(\boldsymbol{x}_1/\lambda) = [(-1-d) \ -6]^T$ and $(\boldsymbol{x}_2/\lambda) = [(1-d) \ -6]^T$.

versus SNR for the two targets being considered, both for FL and BA models. It is apparent that, as the SNR increases, the theoretical results tightly approximate the MC-based ones, with approximations deemed accurate above $\mathrm{SNR} \approx 10\,\mathrm{dB}$. Differently, in Fig. 3, we plot the asymptotic NSD of the three TR-MUSIC variants versus d, where $(\boldsymbol{x}_1/\lambda) = [(-1-d) \ -6]^T$ and $(\boldsymbol{x}_2/\lambda) = [(1-d) \ -6]^T$ (i.e., a rigid shift of the two scatterers), in order to investigate the potentially improved asymptotic stability (viz., NSD) of the generalized spectrum in comparison to Tx and Rx modes. It is apparent that the gain is significant when $d \in (-5, 5)$, while outside this interval the NSD expression is either dominated by Tx or Rx mode, which for the present case $\mathrm{NSD}_{\mathrm{t},k} = 1/\sqrt{11-2} \approx 0.33$ and $\mathrm{NSD}_{\mathrm{r},k} = 1/\sqrt{17-2} \approx 0.26$, with the generalized NSD never above that of $\mathrm{NSD}_{\mathrm{t},k}$ (as dictated from (15)).

V. Conclusion

We provided an asymptotic (high-SNR) analysis of TR-MUSIC null-spectrum in a noncolocated multistatic setup, by taking advantage of the first-order perturbation of the SVD of the MDM. Three different variants of TR-MUSIC were analyzed (i.e., Tx mode, Rx mode and generalized), based on the characterization of a certain complex-valued Gaussian vector. This allowed to obtain the asymptotic NSD (a measure of null-spectrum stability) of all the three imaging procedures. While similar results as the DOA setup were obtained for Tx and Rx modes, it was shown a clear dependence of generalized null-spectrum NSD on the scatterers and measurement setup. Finally, its potential stability advantage was investigated in comparison to Tx and Rx modes. Future works will analyze mutual coupling, antenna pattern, and polarization effects [35], [36], and propagation in inhomogeneous (random) media [37].

REFERENCES

[1] M. Fink, "Time-reversal mirrors," *J. Phys. D: Appl. Phys.*, vol. 26, no. 9, pp. 1333–1350, 1993.

[2] D. Cassereau and M. Fink, "Time-reversal of ultrasonic fields. III. Theory of the closed time-reversal cavity," *IEEE Trans. Ultrason., Ferroelectr., Freq. Control*, vol. 39, no. 5, pp. 579–592, Sep. 1992.

[3] G. Micolau, M. Saillard, and P. Borderies, "DORT method as applied to ultrawideband signals for detection of buried objects," *IEEE Trans. Geosci. Remote Sens.*, vol. 41, no. 8, pp. 1813–1820, Aug. 2003.

[4] L. Li, W. Zhang, and F. Li, "A novel autofocusing approach for real-time through-wall imaging under unknown wall characteristics," *IEEE Trans. Geosci. Remote Sens.*, vol. 48, no. 1, pp. 423–431, Jan. 2010.

[5] M. D. Hossain, A. S. Mohan, and M. J. Abedin, "Beamspace time-reversal microwave imaging for breast cancer detection," *IEEE Antennas Wireless Propag. Lett.*, vol. 12, pp. 241–244, 2013.

[6] C. Prada, S. Manneville, D. Spoliansky, and M. Fink, "Decomposition of the time reversal operator: Detection and selective focusing on two scatterers," *J. Acoust. Soc. Amer.*, vol. 99, no. 4, pp. 2067–2076, 1996.

[7] A. J. Devaney, "Time reversal imaging of obscured targets from multistatic data," *IEEE Trans. Antennas Propag.*, vol. 53, no. 5, pp. 1600–1610, May 2005.

[8] E. A. Marengo and F. K. Gruber, "Subspace-based localization and inverse scattering of multiply scattering point targets," *EURASIP J. Adv. Signal Process.*, 2007, pp. 1–16.

[9] E. A. Marengo, F. K. Gruber, and F. Simonetti, "Time-reversal MUSIC imaging of extended targets," *IEEE Trans. Image Process.*, vol. 16, no. 8, pp. 1967–1984, Aug. 2007.

[10] R. Schmidt, "Multiple emitter location and signal parameter estimation," *IEEE Trans. Antennas Propag.*, vol. 34, no. 3, pp. 276–280, Mar. 1986.

[11] M. Kaveh and A. Barabell, "The statistical performance of the MUSIC and the minimum-norm algorithms in resolving plane waves in noise," *IEEE Trans. Acoust., Speech, Signal Process.*, vol. 34, no. 2, pp. 331–341, Apr. 1986.

[12] B. Friedlander, "A sensitivity analysis of the MUSIC algorithm," *IEEE Trans. Acoust., Speech, Signal Process.*, vol. 38, no. 10, pp. 1740–1751, Oct. 1990.

[13] B. Porat and B. Friedlander, "Analysis of the asymptotic relative efficiency of the MUSIC algorithm," *IEEE Trans. Acoust., Speech, Signal Process.*, vol. 36, no. 4, pp. 532–544, Apr. 1988.

[14] P. Stoica and A. Nehorai, "MUSIC, maximum likelihood, and Cramér-Rao bound," *IEEE Trans. Acoust., Speech, Signal Process.*, vol. 37, no. 5, pp. 720–741, May 1989.

[15] F. Li and R. J. Vaccaro, "Analysis of min-norm and MUSIC with arbitrary array geometry," *IEEE Trans. Aerosp. Electron. Syst.*, vol. 26, no. 6, pp. 976–985, Nov. 1990.

[16] A. L. Swindlehurst and T. Kailath, "A performance analysis of subspace-based methods in the presence of model errors—Part I: The MUSIC algorithm," *IEEE Trans. Signal Process.*, vol. 40, no. 7, pp. 1758–1774, Jul. 1992.

[17] A. Ferréol, P. Larzabal, and M. Viberg, "On the asymptotic performance analysis of subspace DOA estimation in the presence of modeling errors: Case of MUSIC," *IEEE Trans. Signal Process.*, vol. 54, no. 3, pp. 907–920, Mar. 2006.

[18] A. Ferréol, P. Larzabal, and M. Viberg, "On the resolution probability of MUSIC in presence of modeling errors," *IEEE Trans. Signal Process.*, vol. 56, no. 5, pp. 1945–1953, May 2008.

[19] A. Ferréol, P. Larzabal, and M. Viberg, "Statistical analysis of the MUSIC algorithm in the presence of modeling errors, taking into account the resolution probability," *IEEE Trans. Signal Process.*, vol. 58, no. 8, pp. 4156–4166, Aug. 2010.

[20] D. Ciuonzo, G. Romano, and R. Solimene, "On MSE performance of time-reversal MUSIC," in *Proc. IEEE 8th Sensor Array Multichannel Signal Process. Workshop*, Jun. 2014, pp. 13–16.

[21] D. Ciuonzo, G. Romano, and R. Solimene, "Performance analysis of time-reversal MUSIC," *IEEE Trans. Signal Process.*, vol. 63, no. 10, pp. 2650–2662, May 2015.

[22] G. Shi and A. Nehorai, "Cramér-Rao bound analysis on multiple scattering in multistatic point-scatterer estimation," *IEEE Trans. Signal Process.*, vol. 55, no. 6, pp. 2840–2850, Jun. 2007.

[23] J. Choi and I. Song, "Asymptotic distribution of the MUSIC null spectrum," *IEEE Trans. Signal Process.*, vol. 41, no. 2, pp. 985–988, Feb. 1993.

[24] F. Li, H. Liu, and R. J. Vaccaro, "Performance analysis for DOA estimation algorithms: Unification, simplification, and observations," *IEEE Trans. Aerosp. Electron. Syst.*, vol. 29, no. 4, pp. 1170–1184, Oct. 1993.

[25] D. Ciuonzo and P. Salvo Rossi, "On the asymptotic distribution of time-reversal MUSIC null spectrum," *Elsevier Digital Signal Process.*, submitted for publication.

[26] E. G. Asgedom, L.-J. Gelius, A. Austeng, S. Holm, and M. Tygel, "Time-reversal multiple signal classification in case of noise: A phase-coherent approach," *J. Acoust. Soc. Amer.*, vol. 130, no. 4, pp. 2024–2034, 2011.

[27] M. E. Yavuz and F. L. Teixeira, "On the sensitivity of time-reversal imaging techniques to model perturbations," *IEEE Trans. Antennas Propag.*, vol. 56, no. 3, pp. 834–843, Mar. 2008.

[28] A. C. Fannjiang, "The MUSIC algorithm for sparse objects: A compressed sensing analysis," *Inverse Probl.*, vol. 27, no. 3, 2011, Art. no. 035013.

[29] H. Krim and M. Viberg, "Two decades of array signal processing research: The parametric approach," *IEEE Signal Process. Mag.*, vol. 13, no. 4, pp. 67–94, Jul. 1996.

[30] G. Shi and A. Nehorai, "Maximum likelihood estimation of point scatterers for computational time-reversal imaging," *Commun. Inf. Syst.*, vol. 5, no. 2, pp. 227–256, 2005.

[31] G. W. Stewart, "Error and perturbation bounds for subspaces associated with certain eigenvalue problems," *SIAM Rev.*, vol. 15, no. 4, pp. 727–764, 1973.

[32] J. Liu, X. Liu, and X. Ma, "First-order perturbation analysis of singular vectors in singular value decomposition," *IEEE Trans. Signal Process.*, vol. 56, no. 7, pp. 3044–3049, Jul. 2008.

[33] D. S. Bernstein, *Matrix Mathematics: Theory, Facts, and Formulas*. Princeton, NJ, USA: Princeton Univ. Press, 2009.

[34] P. J. Schreier and L. L. Scharf, *Statistical Signal Processing of Complex-Valued Data: The Theory of Improper and Noncircular Signal*. Cambridge, U.K.: Cambridge Univ. Press, 2010.

[35] K. Agarwal and X. Chen, "Applicability of MUSIC-type imaging in two-dimensional electromagnetic inverse problems," *IEEE Trans. Antennas Propag.*, vol. 56, no. 10, pp. 3217–3223, Oct. 2008.

[36] R. Solimene and A. Dell'Aversano, "Some remarks on time-reversal MUSIC for two-dimensional thin PEC scatterers," *IEEE Geosci. Remote Sens. Lett.*, vol. 11, no. 6, pp. 1163–1167, Jun. 2014.

[37] A. E. Fouda and F. L. Teixeira, "Statistical stability of ultrawideband time-reversal imaging in random media," *IEEE Trans. Geosci. Remote Sens.*, vol. 52, no. 2, pp. 870–879, Feb. 2014.